Low-Polarization-Dependent Silica Waveguide Monolithically Integrated on SOI Photonic Platform

Hidetaka Nishi, *Member, OSA*, Tai Tsuchizawa, Hiroyuki Shinojima, Toshifumi Watanabe, Sei-Ichi Itabashi, Rai Kou, *Member, IEEE*, Hiroshi Fukuda, *Member, IEEE*, and Koji Yamada, *Member, IEEE*

***Abstract*—We developed a low-polarization-dependent silica-based waveguide, which can be monolithically integrated with a silicon (Si) waveguide device on a silicon-on-insulator (SOI) substrate. For the monolithic integration, silica-based materials must be deposited at low temperature in order not to damage Si waveguide devices. Due to this low-temperature fabrication method, however, the silica films exhibit high residual stress, resulting in high material birefringence. In order to compensate for this birefringence, we introduce a multi-layer core structure. First, we design the structure taking the monolithic integration with the Si waveguide devices into account. Then, the designed waveguides and arrayed-waveguide gratings (AWGs) are fabricated using low-temperature fabrication processes. Next, we experimentally confirm that the waveguide exhibits low waveguide birefringence. In addition, we monolithically integrate the AWG and Si waveguide devices.**

***Index Terms*—Birefringence, monolithic integation, polarization, Si photonics, SiO_x waveguide.**

I. Introduction

Silicon (Si) photonics technology has the potential to provide highly integrated and cost-effective photonic-electronic integrated devices. In this technology, photonic waveguide devices are mainly composed of Si waveguides fabricated on an Si-on-insulator (SOI) substrate. By utilizing the strong optical confinement of Si waveguides with submicrometer dimensions, ultrasmall wavelength filters have been developed [1], [2].

However, the strong optical confinement also has a harmful effect. Namely, the effective refractive index of the Si wire waveguide significantly changes due to the error of several nanometers in the fabrication of the Si core. Therefore, a filter device exhibits large polarization dependence even if the core geometry is designed so that birefringence is eliminated. In addition, Si wire waveguide devices exhibit higher propagation loss and temperature dependence than silica-based ones. These issues are critical for the implementation of Si photonics devices to loss-, temperature-, and polarization-sensitive applications, such as in long-distance optical telecommunications networks. To resolve these issues, instead of the Si wire waveguide, a Si waveguide with micrometer core dimensions [3] and silicon-nitride (SiN) [4] and silicon-oxide (SiO_x) waveguides [5]–[7] have been examined and successfully integrated on the SOI photonic platform.

In particular, SiO_x waveguides are promising because they exhibit low propagation loss and a low thermo-optic coefficient. For the monolithic integration, the SiO_x film must be deposited at low temperature in order not to damage Si waveguide devices. Recently, we have developed a low-loss SiO_x waveguide that can be fabricated at low temperature [5]. However, the films prepared by this low-temperature deposition method contain compressive stress of several hundred mega-pascals. Consequently, the SiO_x waveguide exhibits waveguide birefringence on the order of 10^{-3}, which is about ten times larger than that of silica-based waveguides [8].

A lot of methods for reducing waveguide birefringence have been reported, all of which are based on one of two strategies. One is stress reduction, which involves the addition of stress-releasing grooves [9], [10], making a ridge-shaped undercladding [8], and adjusting thermal expansion coefficient [11]. The other is the addition of inverse birefringence and compensation, which involves adjustment of the aspect ratio of the core geometry [12], deposition of a stress inducer [13], and insertion of a high-index layer into the bottom of the core [14].

In this paper, we report an SiO_x waveguide with a multi-layer core structure. First, we design the structure and confirm that the large birefringence of the order of 10^{-3} can be compensated. In addition, we optimize the structure taking the integration with the Si waveguide devices into account. Next, we actually fabricate the waveguides and arrayed-waveguide gratings (AWGs) using low-temperature fabrication methods. The fabrication process is highly compatible with the complementary metal-oxide semiconductor (CMOS) process. Then, we evaluate the fabricated devices, and confirm the feasibility and validity of the multi-layer core design to reduce the waveguide birefringence. Finally, we monolithically integrate them with the Si waveguide devices.

II. Design

Fig. 1 is a schematic cross section of a multi-layer core structure. For the monolithic integration, a buried-oxide (BOX) layer of an SOI substrate is used as an undercladding. The SiO_x core and SiO_2 overcladding are fabricated on this BOX layer [5]. The compressive stress in the fabricated film is higher in the horizontal direction than in the vertical direction to the substrate

Manuscript received December 18, 2012; revised February 14, 2013 and March 17, 2013; accepted March 21, 2013. Date of publication April 04, 2013; date of current version May 15, 2013.

H. Nishi, T. Tsuchizawa, R. Kou, H. Fukuda, and K. Yamada are with NTT Microsystem Integration Laboratories and Nanophotonics Center, Nippon Telegraph and Telephone Corporation, Kanagawa 243-0198, Japan (e-mail: nishi.hidetaka@lab.ntt.co.jp).

H. Shinojima is with Kurume National College of Technology, Fukuoka 830-8555, Japan.

T. Watanabe and S. Itabashi are with NTT Advanced technology corporation, Kanagawa 243-0198, Japan.

Digital Object Identifier 10.1109/JLT.2013.2256880

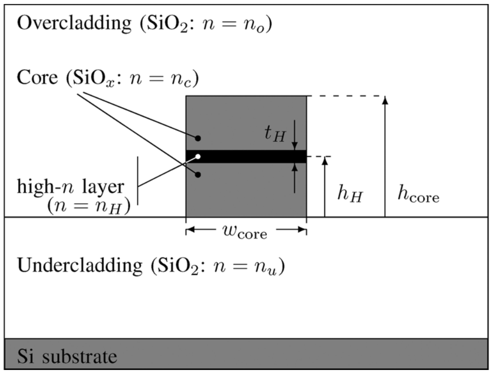

Fig. 1. Schematic cross section of SiO_x waveguide with a multi-layer core structure.

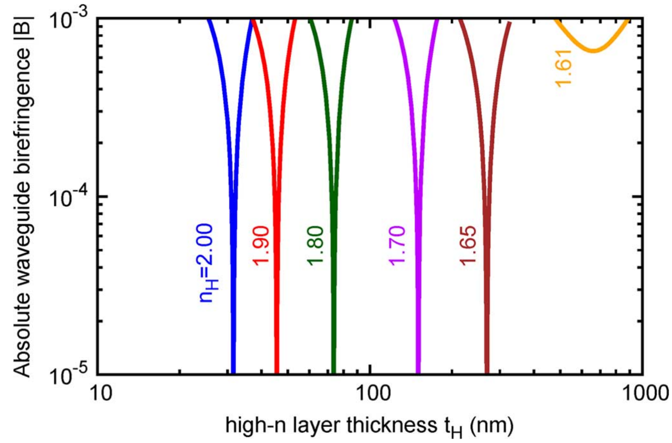

Fig. 2. Calculated t_H dependence of absolute value of B for vaious values of n_H. h_H was set to 1.5 μm.

plane, and makes the refractive index in the vertical direction, n_{vert}, higher than that of horizontal direction, n_{hor} [15]. Here, we define material birefringence Δn as $\Delta n = n_{\mathrm{hor}} - n_{\mathrm{vert}}$. As we noted above, $\Delta n < 0$. This negative Δn leads to a higher effective refractive index for the transverse-magnectic (TM) mode, n_{TM}, than for the transverse-electric (TE) mode, n_{TE}. Here, we define waveguide birefringence B as $B = n_{\mathrm{TE}} - n_{\mathrm{TM}}$. In order to compenste B, in this work, a high-refractive-index (high-n) layer is inserted into the SiO_x core as shown in Fig. 1. By the insertion of the high-n layer, the negative Δn still remains in the SiO_x core and SiO_2 overcladding, but positive waveguide birefringence occurs due to the structural asymmetry because the TE mode is easier to confine in a horizontal high-n layer than the TM mode. Therefore, even though negative Δn remains in the SiO_x layer, this positive structural birefringence enables compensation of negative B of the waveguide.

In designing the multi-layer core structure, we use the following three parameters: the refractive index of the high-n layer n_H, thickness of the high-n layer t_H, and insertion position of the high-n layer h_H, which are defined in Fig. 1. The other parameters were the same as in our developed waveguide design [5]. Namely, h_{core} and w_{core}, which were both set to 3.0 μm, and n_o, n_c, and n_u, which were set to 1.468, 1.505, and 1.444, respectively. Before the design is started, Δn in the SiO_x core and SiO_2 overcladding should be understood. We estimate Δn by the following procedure. First, we measured the polarization-dependent wavelength shift, $\mathrm{PD}\lambda = \lambda_{\mathrm{TE}} - \lambda_{\mathrm{TM}}$, of an AWG based on SiO_x waveguides with a monolayer core. λ_{TE} and λ_{TM} are center wavelengths of the AWG passband for each polarization. The AWG in this work consists of SiO_x waveguides and has 16 channels with 200-GHz spacing. The number of arrayed waveguides is 64. The waveguides have a minimum bending radius of 500 μm and path-length difference of 55.4 μm. Focal length of the slab region is 1.75 mm. The measured $\mathrm{PD}\lambda$ is -4.39 nm. Next, we calculated B by substituting the obtained $\mathrm{PD}\lambda$ into following equation;

$$\mathrm{PD}\lambda = \frac{B}{n_{\mathrm{TE}}}\lambda_{\mathrm{TE}}. \quad (1)$$

After that, we estimate Δn from the obtained B. We repeatedly calculate the n_{TE} and n_{TM} with varying Δn so that the B becomes the value calculated above. Here, for the calculation, we use a commercial mode solver based on the film-mode-matching method [16], [17] and assume that Δn is homogeneous and independent of thickness in the core and overcladding layers. Finally, we find that Δn is -4.4×10^{-3}.

A. Refractive Index of the High-n Layer

We begin with the design of n_H. For the calculation, the wavelength is set to 1550 nm. Fig. 2 shows the calculated t_H dependence of $|B|$ for various n_H's. Here, h_H was set to 1.5 μm. For simplification, we considered only the fundamental modes for the both polarizations. As shown in Fig. 2, with n_H of over 1.65, we can obtain $|B|$ of less than 10^{-5}. As n_H becomes higher, optimum t_H becomes smaller. Meanwhile, with n_H of 1.61, we can not obtain $|B|$ of less than 6.55×10^{-4}. This is due to the birefringence in the high-n layer. As the n_H becomes low, the required t_H becomes large and the propagation mode becomes more confined in the high-n layer. With this strong confinement, the positive structural birefringence decreases and becomes too small to compensate the negative Δn in the SiO_x material. In addition, the effective indexes then significantly reflect the influence of Δn in the high-n layer. In this calculation, we assume that Δn is negative and homogeneous in the whole core and overcladding region. Hence, when we set n_H to 1.61, the B can not be compensated. For a more accurate design with n_H of a relatively low value, a table of Δn in the high-n layer may be required, which would vary depending on the n_H value, material, and fabrication method.

In contrast, with n_H of a relatively high value, we do not need to carefully consider the uncertainty of Δn in the high-n layer. Therefore, in order to simply confirm the validity of the multi-layer core structure, it is favorable to choose a high n_H material. In this work, we choose SiN as a high-n material. SiN has a relatively high refractive index and can be fabricated at low temperature by CMOS-compatible processes. The refractive index of the SiN we fabricated is 1.90, slightly low compared with the commonly reported value of about 2.0 [18]–[20]. The difference occurs because of differences in the fabrication methods. We will describe the detail of our SiN fabrication later in the fabrication section.

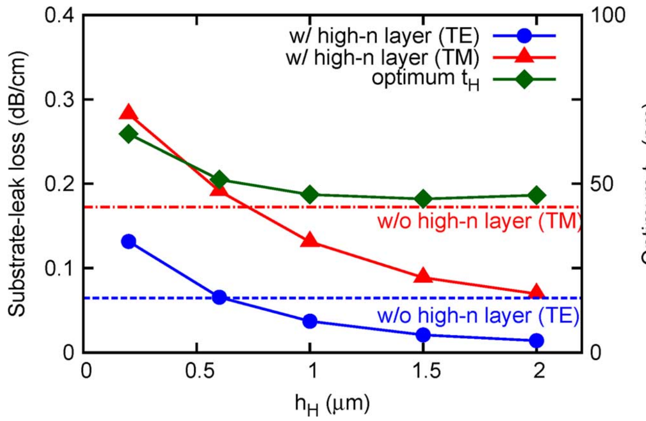

Fig. 3. Calculated h_H dependence of substrate-leak loss for each polarization (left axis). t_H was set as the optimum value for each insertion position h_H (right axis). n_H was set to 1.90.

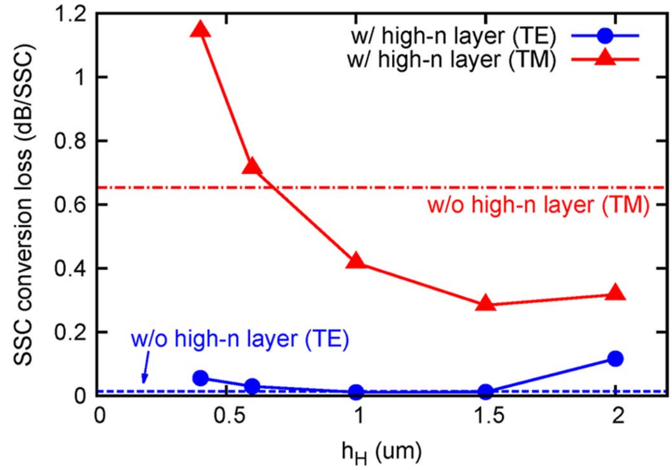

Fig. 4. Calculated h_H dependence of SSC conversion loss.

B. Thickness and Inserting Position of the High-n Layer

Next, we design t_H and h_H taking into account two issues about loss performance. One is optical leakage to the Si bottom substrate of the SOI wafer. Propagation modes of the SiO_x waveguide are confined more weakly and more sensitively to substrate leakage than those of Si wire waveguides. In addition, commercial SOI wafers for use in Si photonics often have a BOX layer with a thickness of less than 3 μm, which is not thick enough for an SiO_x waveguide to isolate propagation modes from substrate leakage. Therefore, substrate-leak loss can easily increase. To cope with this issue, our approach is set h_H as high as possible to separate the propagation mode from the Si substrate.

To confirm the validity of this approach, we calculated the substrate-leak loss with h_H as a parameter using the mode solver. For the substrate-leak loss calculation, we placed a thin Si layer under the 3-μm-thick BOX layer and set a transparent boundary condition at the bottom edge of the computation window. The optimum t_H to achieve birefringence compensation varies depending on h_H. So, for each h_H, we calculated the optimum t_H in advance, and then calculated the substrate-leak loss using each optimum t_H.

Fig. 3 shows the calculated h_H dependence of substrate-leak loss for each polarization (left axis). The optimum t_H for each h_H is also shown (right axis). The n_H was set to 1.90. As we expected, the substrate-leak loss decreases as h_H increases for both polarizations. As a reference, the substrate-leak loss of the SiO_x waveguide without the high-n layer (what we call “the monolayer-core waveguide” hereafter) is also shown. With h_H of over 1 μm, the substrate-leak loss becomes lower than that of the monolayer-core waveguide for both polarizations. Owing to the reduction of the substrate-leak loss, the polarization-dependent loss (PDL) is also suppressed. Here, the PDL is defined as the difference of the losses between polarizations. With h_H of over 1 μm, the PDL per unit length becomes less than 0.1 dB/cm. We might slightly reduce the substrate-leak loss by setting h_H more higher. Meahwhile, the setting h_H too high seems to have an adverse influence on the other issue: conversion loss at a spot-size converter (SSC).

From the viewpoint of monolithic integration with the Si waveguide, the SSC is indispensable. In this work, we consider an SSC consisting of an Si taper and the covering SiO_x core [5]. With this SSC, conversion loss may change depending on h_H. Therefore, to develop a low-loss SSC, we calculate the SSC conversion loss with h_H as a parameter. Fig. 4 shows the h_H dependence of SSC conversion loss calculated by the eigenmode-expansion method [17]. In each calculation, we set the following dimensions in common: Si-taper tip width of 60 nm, which is expanded to 300 nm with a 300-μm-long taper and connected to the Si-wire-waveguide core; and taper height of 300 nm, which is consistent with the Si wire waveguide. The n_H was set to 1.90, and t_H was set in the same way as that in the substrate-leak-loss calculation. In Fig. 4, we also show the conversion losses of an SSC consisting of the monolayer-core waveguide as a reference.

First, we discuss the conversion loss for the TM mode, which exhibits a higher value than the TE mode. In the SSC consisting of the monolayer-core waveguide, this high TM loss originates in mode mismatch at the interface between the SiO_x waveguide and the Si taper tip. Because of the Si height of 300 nm, the TM mode at the Si-taper tip is well confined in the Si. On the other hand, by narrowing the Si-tip width, the TE mode is less confined to the Si and leaks out to the covering SiO_x core. So, the mode mismatch is small. Therefore, the PDL is as high as over 0.6 dB with the monolayer-core SiO_x waveguide. One way to reduce the loss for the TM mode and PDL is to decrease the Si height. However, from the viewpoint of polarization dependence in Si waveguide devices, it may happen that the Si height must be set to the designed value and should not be lower. For example, an Si variable optical attenuator must be fabricated with a designed Si height to make it polarization independent [21].

Fortunately, the high-n layer insertion helps to weaken this strong confinement of the TM mode and decrease the mode mismatch. As shown in Fig. 4, the SSC conversion loss for the TM mode decreases as h_H increases from 0.4 to 1.5 μm, and it becomes lower than that with the monolayer-core with h_H of over 1 μm. This is because the mode mismatch decreases as h_H increases, exhibiting the minimum value of 0.28 dB/SSC with h_H

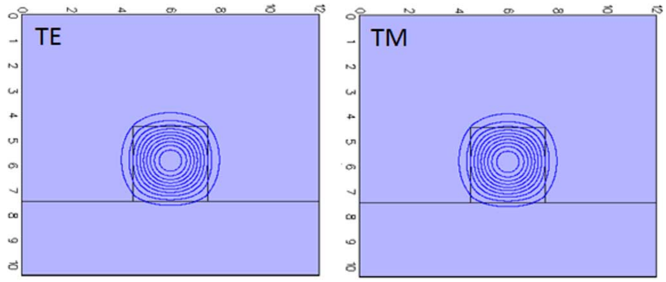

(a)

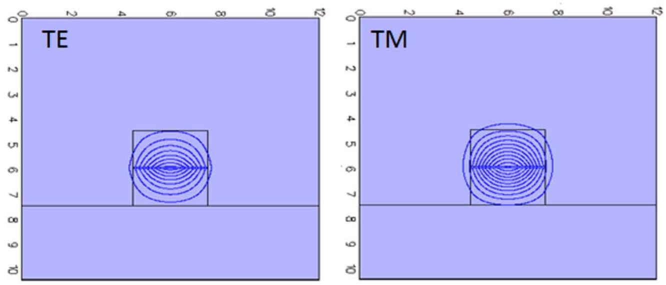

(b)

Fig. 5. Calculated mode-field profiles for both polarizations. (a) is for without high-n layer and (b) is for with high-n layer. n_H, h_H, and t_H are set to 1.90, 1.5 μm, and 45.5 nm, respectively.

of 1.5 μm. Meanwhile, as h_H increases from 1.5 μ to 2 μm, the SSC conversion loss increases. This also originates in the mode mismatch. For the TE mode, on the other hand, the SSC conversion loss is less than 0.1 dB with h_H of 1.5 μm. The PDL is less than 0.3 dB/SSC. Thus, taking the substrate-leak loss and the SSC conversion loss into account, we concluded that h_H of 1.5 μm is the best. With h_H of 1.5 μm, the calculated optimum t_H is 45.5 nm. Fig. 5 shows caclucated mode-field profiles for both polarizations. Using the measurement results for the fabricated device, we will finely adjust the t_H and optimize it to obtain the minimum $|B|$.

III. Fabrication

First, on the 3-μm-thick SiO_2 layer, we deposited SiO_x and SiN layers with the designed thickness using a low-temperature fabrication method based on plasma-enhanced chemical vapor deposition (PECVD) technology with electron-cyclotron-resonance (ECR) plasma [5], [22], [23]. The refractive index of the SiO_x layer was adjusted to be 1.51 by changing the gas flow ratio of SiH_4 and O_2 [5]. For the deposition of the SiN layer, we used an SiH_4 and N_2 gas mixture. Owing to this fabrication method, the SiN consists of Si, nitrogen, and hydrogen. During the deposition, the N_2 gas flow rate was high enough to saturate the nitrogen content in the film. The obtained refractive index is 1.90 at 1550 nm. As we mentioned in the design section, this index is slightly lower than that of commonly reported SiN films because of the fabrication method. In fact, similar low refractive indexes have also been obtained by the low-temperature ECR PECVD method [23]. Next, we defined the waveguide's core and AWG pattern using ultraviolet lithography and plasma reactive-ion etching. Finally, we deposited the SiO_2 overcladding, also using ECR PECVD. These fabrication processes were performed at low temperature of less than 200 degrees Celsius. In

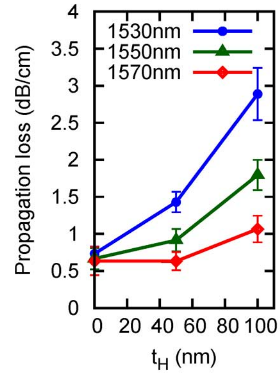

(a)

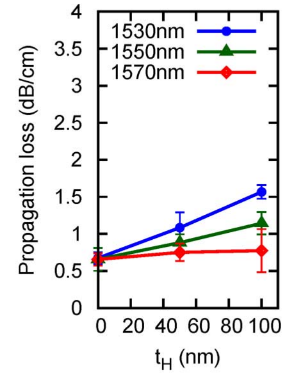

(b)

Fig. 6. t_H dependence of propagation loss at 1530, 1550, and 1570 nm. Input polarizations are TE for (a) and TM for (b).

addition, the processes mentioned above were introduced for the monolithic integraton of an SiO_x AWG and Si variable optical attenuators (VOAs), and we fabricated an AWG-VOA integrated device. The detailed integration process is reported in [5], [24]. The fabricated chips were diced to couple the light from the facet.

IV. Experimental Results and Discussion

A. SiO_x Waveguide With the Multi-Layer Core

First, we measured propagation losses of fabricated waveguides with various t_H values. The propagation loss was estimated from the slope of the relationship between transmittance and waveguide length. The transmittance was obtained as follows: We measured the transmission spectra using a C-band amplified-spontaneous-emission (ASE) light source and an optical spectrum analyzer (OSA). The light from the ASE source was adjusted for optimum polarization using an in-line polarization controller and put into a thermally-fused high-numerical-aperture (high-NA) fiber with mode-field diameter of 4.1 μm. The high-NA fiber was butt-coupled to the facet of the fabricated chip with index-matching oil. The output light was put into the OSA in a similar way to the input. The measured transmitted power spectrum was normalized by a fiber-to-fiber power spectrum. The transmittance was evaluated at 1530, 1550, and 1570 nm. At each wavelength, the transmittance was calculated from the averaged value within each center wavelength ± 1 nm.

Fig. 6 shows the relationship between t_H and propagation loss. For the monolayer-core waveguide, the propagation losses at 1550 nm for the TE and TM modes were 0.67 and 0.66 dB/cm, respectively. By the insertion of the high-n layer, additional loss emerged. This additional loss increases as t_H increases. With t_H of 50 nm, the propagation losses were 0.91 and 0.88 dB/cm for the TE and TM modes, respectively. As the origin of additional loss, we consider absorption loss in the SiN layer. Hydrogen-containing SiN film has broad N-H absorption centered at around 1500 nm [25]. Of course, the loss due to this N-H absorption loss increases as t_H increases. In addition, regarding wavelength dependence under the same t_H, the measured propagation loss was higher at 1530 nm than at 1570 nm. This result is consistent with the fact that the N-H absorption loss is higher at 1530 nm than at 1570 nm due to the long absorption tail.

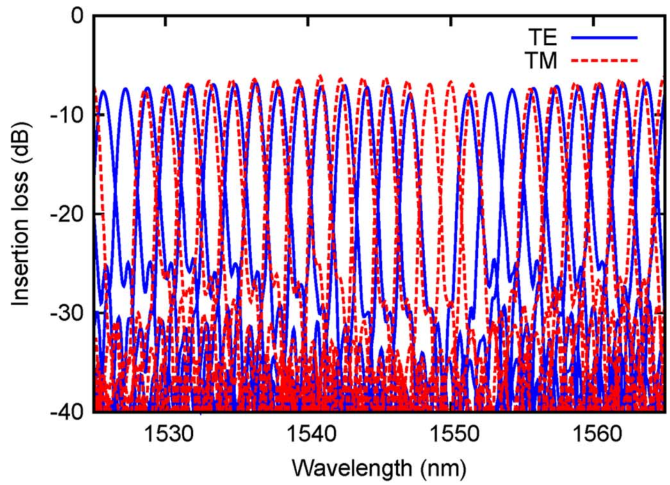

(a)

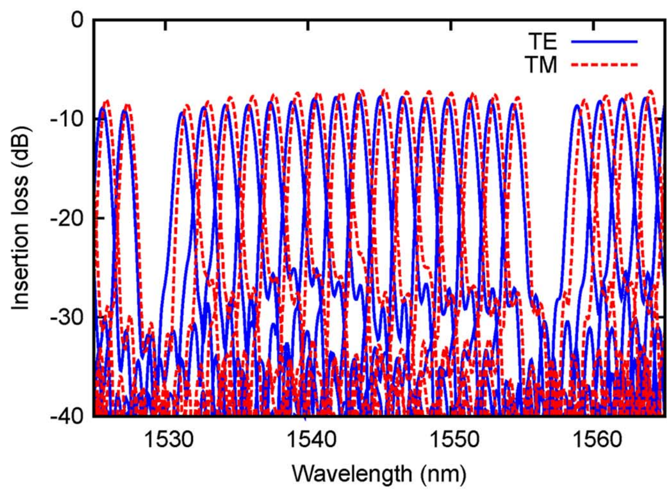

(b)

Fig. 7. Spectra of fabricated AWGs. (a) and (b) correspond to t_H of 0 and 40 nm, respectively.

Moreover, regarding polarization dependence under the same t_H, the propagation loss for the TE mode was higher than that for the TM mode. This is also consistent with the fact that the TE mode is more confined in the high-n layer than the TM mode as we mentioned in the design section. Therefore, we concluded that the additional loss occurred because of absorption loss at the SiN layer. Unfortunately, the effect of the high-n layer insertion to suppress the substrate-leak loss was not observed explicitly because the N-H absorption loss was too high to confirm that in the C-band. A promising way to avoid this additional loss is to use hydrogen-free SiN film. For example, we could fabricate such a film by Si sputtering in N_2 atmosphere [26] instead of the PECVD deposition used in this work.

B. AWG Based on SiO_x Waveguide With Multi-Layer Core

Next, we confirm birefringence compensation through AWGs measurements. Fig. 7 shows measured spectra for fabricated SiO_x AWGs. The AWG with the monolayer-core waveguide ($t_H = 0$ nm), shown in Fig. 7(a), exhibits large $\mathrm{PD}\lambda$ of -4.39 nm on average. On the other hand, we obtained $\mathrm{PD}\lambda$ of -0.31 nm from the AWG with t_H of 40 nm, as shown in Fig. 7(b).

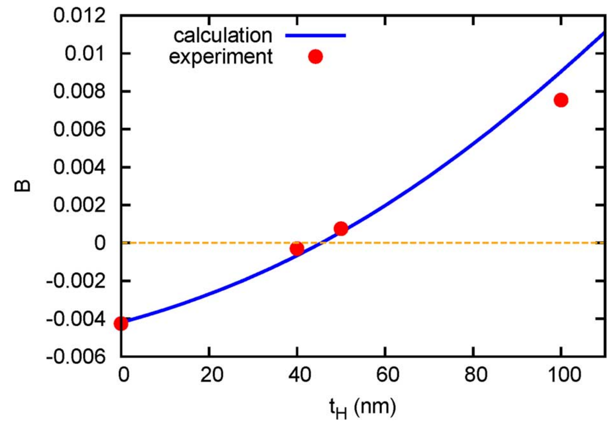

Fig. 8. Measured t_H dependence of B and comparison with calculation result.

Here, birefringence compensation by insertion of the high-n layer is clearly confirmed. Fig. 8 shows the calculated and measured relationships between t_H and B. As t_H increases, B increases and changes from negative to positive between $t_H = 40$ and 50 nm. The experimental results exhibit the same tendency and well agree with the calculation. The error between the experimental and calculated value is relatively big with t_H of 100 nm. We guess this is due to the assumption in the calculation as we mentioned in the design section. In addition, the estimated Δn in the SiO_x and SiO_2 layer might be varied by the insertion of the high-n layer, and this effect might become apparent with large t_H. The obtained minimum B was 3.0×10^{-4} when t_H was 40 nm. A further decrease of $|B|$ will be achieved by precise control of t_H.

Here, we discuss the PDL of the AWGs. As shown in Fig. 7(b), the PDL was less than 0.9 dB for all channels even though a 40-nm SiN layer was inserted. Of this PDL, 0.6 dB originates from additional loss of the multi-layer core SiO_x waveguide. This PDL will be reduced by using the hydrogen-free SiN as we mentioned above. Residual PDL of 0.3 dB may occur at the fiber coupling. In fact, with the insertion of high-n layer, the mode mismatch at the interface between the high-NA fiber and SiO_x waveguide increases. We guess that this mode mismatch leads to the PDL at the fiber coupling. As future work, we will further decrease the PDL by introducing a specific design for the fiber coupling [27].

C. Monolithic Integration of SiO_x Waveguide With Multi-Layer Core and Si VOAs Using SSC

Finally, we monolithically integrated this multi-layer core SiO_x waveguide and the Si-wire-waveguide device. Fig. 9 is a top-view image of a fabricated device. An SiO_x AWG is integrated with Si VOAs using SSCs. The details of the integration structure are described in [5] and [24]. The Si VOA is based on a Si wire waveguide with a p-i-n carrier-injection structure and is designed for polarization-independent operation [21]. The SiN layer was fabricated with t_H of 42 nm. This value was obtained from interpolation of the experimental results on the Fig. 8 so that B became zero.

The transmission spectra of a single channel of a fabricated device are shown in Fig. 10(a). In order to obtain this spectra, we input constant optical power and applied bias voltage to

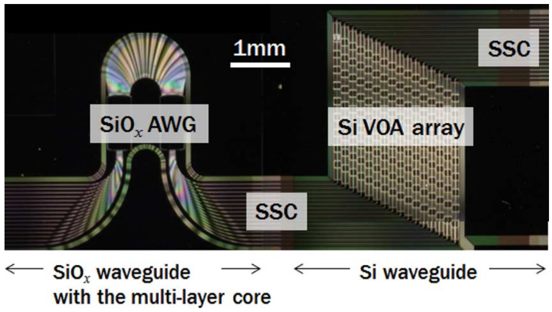

Fig. 9. Top-view image of fabricated AWG-VOA integrated device.

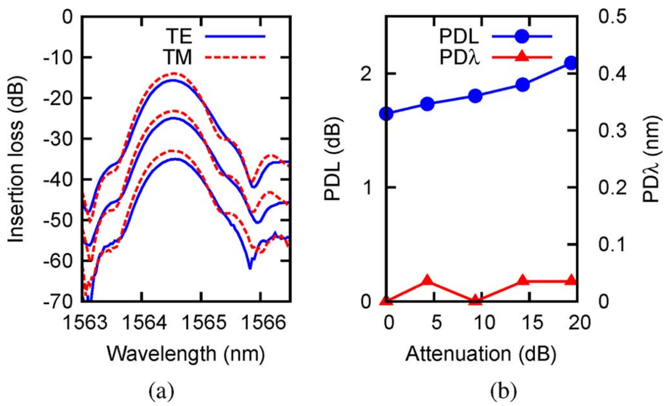

Fig. 10. (a) Transmission spectra of an integrated device consisting of an SiO_x AWG and Si VOAs. Three transmission levels correspond to 0-, 10-, and 20-dB attenuation of the VOA. (b) The VOA attenuation dependence of the PDL (left axis) and the $PD\lambda$ (right axis).

the Si VOA in three levels to obtain attenuation of 0, 10, 20 dB. On each attenuation level, the applied bias was the same for the TE and TM modes. We confirmed that the fabricated AWG and VOA operated well. The multi-layer core SiO_x waveguide was successfully integrated without thermal damage to the Si waveguide devices. In addition, apparently, the polarization dependence of the fabricated AWG-VOA device is low. Fig. 10(b) shows VOA-attenuation dependence of the PDL and $PD\lambda$. $PD\lambda$ is less than 0.1 nm regardless of the VOA attenuation. This result demonstrates the validity of the multi-layer core SiO_x waveguide. In addition, the precise control of t_H enables us to obtain significantly low $PD\lambda$.

Another issue is the PDL, which is 1.6 dB without the VOA attenuation. The PDL was estimated at the wavelength of 1564.53 nm. Of this PDL, 0.8 dB originates from the propagation loss of the multi-layer core SiO_x waveguide. The measured propagation losses of the integrated SiO_x waveguide for the TE and TM modes were 1.5 and 1.1 dB/cm, respectively. In comparison with the stand-alone waveguide, the propagation loss evidently increases. The high propagation loss leads to the high PDL of the SiO_x waveguide. We guess this is due not to the multi-layer core structure but to the monolithic-integration process for the Si VOAs. We will decrease the propagation loss and the PDL by improving the integration process. Besides, the PDL at the SSC was estimated to be only about 0.1 dB. We confirmed that the multi-layer core structure does not degrade the PDL at the SSC. The residual PDL of about 0.8 dB occurred at the Si waveguide, diffraction in the AWG, and the fiber coupling. Among them, the fiber coupling is the main PDL source. The PDL was 0.5 dB. This value differs 0.2 dB from the stand-alone AWG measurement. We guess the difference emerges because of measurement error. In order to decrease the PDL at the fiber coupling, the careful design of the waveguide structure at the fiber-interface is promising as we mentioned about the stand-alone SiO_x AWG.

V. Conclusion

We developed an SiO_x waveguide with low birefringence using a multi-layer core structure. The SiO_x waveguide can be fabricated at low temperature and monolithically integrated with Si waveguide devices on the SOI photonic platform. Towards implementation of the Si photonics devices for applications such as telecommunications that require low-loss, thermal stability, and polarization insensitivity, the SiO_x waveguide provides leverage.

Acknowledgment

The authors thank S. Park and S. Mutoh for their helpful support and discussions.

References

[1] K. Sasaki, F. Ohno, A. Motegi, and T. Baba, "Arrayed waveguide grating of 70 × 60 μm^2 size based on Si photonic wire waveguides," *Electron. Lett.*, vol. 41, p. 801, 2005.

[2] W. Bogaerts, P. Dumon, D. V. Thourhout, D. Taillaert, P. Jaenen, J. Wouters, S. Beckx, V. Wiaux, and R. G. Baets, "Compact wavelength-selective functions in silicon-on-insulator photonic wires," *IEEE J. Sel. Quantum Electron.*, vol. 12, pp. 1394–1401, 2006.

[3] D. Feng, N.-N. Feng, C.-C. Kung, H. Liang, W. Qian, J. Fong, B. J. Luff, and M. Asghari, "Compact single-chip VMUX/DEMUX on the silicon-on-insulator platform," *Opt. Exp.*, vol. 19, no. 7, p. 6125, Mar. 2011.

[4] C. R. Doerr, L. Chen, L. L. Buhl, and Y. Chen, "Eight-channel SiO/Si N/Si/Ge CWDM receiver," *IEEE Photon. Technol. Lett.*, vol. 23, no. 17, pp. 1201–1203, 2011.

[5] T. Tsuchizawa, K. Yamada, T. Watanabe, S. Park, H. Nishi, R. Kou, H. Shinojima, and S. Itabashi, "Monolithic integration of silicon-, germanium-, and silica-based optical devices for telecommunications applications," *IEEE J. Sel. Top. Quantum. Electron.*, vol. 17, pp. 516–525, 2011.

[6] H. Nishi, T. Tsuchizawa, R. Kou, H. Shinojima, T. Yamada, H. Kimura, Y. Ishikawa, K. Wada, and K. Yamada, "Monolithic integration of a silica AWG and Ge photodiodes on Si photonic platform for one-chip WDM receiver," *Opt. Exp.*, vol. 20, no. 8, pp. 9312–9321, Apr. 2012.

[7] R. Kou, H. Fukuda, T. Tsuchizawa, H. Nishi, T. Hiraki, and K. Yamada, "Silicon/silica-hybrid delay line interferometer for DPSK demodulation," in *Proc. IEEE Group IV Photonics 2012 (GFP2012)*, San Diego, CA, USA, 2012.

[8] R. Kasahara, M. Itoh, Y. Hida, T. Saida, Y. Inoue, and Y. Hibino, "Birefringence compensated silica-based waveguide with undercladding ridge," *Electron. Lett.*, vol. 38, p. 1178, 2002.

[9] M. Kawachi, "Silica waveguides on silicon and their application to integrated-optic components," *Opt. Quantum Electron.*, vol. 22, no. 5, pp. 391–416, Sep. 1990.

[10] C. K. Nadler, E. K. Wildermuth, M. Lanker, W. Hunziker, and H. Melchior, "Polarization insensitive, low-loss, low-crosstalk wavelength multiplexer modules," *IEEE J. Sel. Quantum Electron.*, vol. 5, pp. 1407–1412, 1999.

[11] S. Suzuki, S. Sumida, Y. Inoue, M. Ishii, and Y. Ohmori, "Polarisation-insensitive arrayed-waveguide gratings using dopant-rich silica-based glass with thermal expansion adjusted to Si substrate," *Electron. Lett.*, vol. 33, no. 13, p. 1173, 1997.

[12] K. Wörhoff, C. G. H. Roeloffzen, R. M. de Ridder, A. Driessen, and P. V. Lambeck, "Design and application of compact and highly tolerant polarization-independent waveguides," *Journal of Lightwave Technology*, vol. 25, pp. 1276–1283, 2007.

[13] H. Takahashi, Y. Hibino, Y. Ohmori, and M. Kawachi, "Polarization-insensitive arrayed-waveguide wavelength multiplexer with birefringence compensating film," *IEEE Photon. Technol. Lett.*, vol. 5, pp. 707–709, 1993.
[14] K. Wörhoff, B. J. Offrein, P. V. Lambeck, G. L. Bona, and A. Driessen, "Birefringence compensation applying double-core waveguiding structures," *IEEE Photon. Technol. Lett.*, vol. 11, no. 2, pp. 206–208, Feb. 1999.
[15] G. W. Scherer, "Stress-induced index profile distortion in optical waveguides," *Appl. Opt.*, vol. 19, p. 2000, 1980.
[16] A. S. Sudbo, "Film mode matching: a versatile numerical method for vector mode field calculations in dielectric waveguides," *Pure Appl. Opt.*, vol. 2, pp. 211–233, 1993.
[17] Aug. 2012, "FIMMWAVE Version 5.4.1," Photon Design.
[18] L. Chen, C. Doerr, L. Buhl, Y. Baeyens, and R. A. Aroca, "Monolithically integrated 40-wavelength demultiplexer and photodetector array on silicon," *IEEE Photon. Technol. Lett.*, vol. 23, pp. 869–871, 2011.
[19] D. Dai, Z. Wang, J. F. Bauters, M. Tien, M. J. R. Heck, J. Daniel, and J. E. Bowers, "Low-loss Si_3N_4 arrayed-waveguide grating (de) multiplexer using nano-core optical waveguide," *Opt. Exp.*, vol. 19, pp. 940–942, 2011.
[20] H. J. Lee, C. H. Henry, K. J. Orlowsky, R. F. Kazarinov, and T. Y. Kometani, "Refractive-index dispersion of phosphosilicate glass, thermal oxide, and silicon nitride films on silicon," *Appl. Opt.*, vol. 27, p. 4104, 1988.
[21] H. Nishi, T. Tsuchizawa, T. Watanabe, H. Shinojima, K. Yamada, and S. Itabashi, "Compact and polarization-independent variable optical attenuator based on a silicon wire waveguide with a carrier injection structure," *Jpn. J. Appl. Phys.*, vol. 49, no. 4, p. 04DG20, Apr. 2010.
[22] S. Matsuo and M. Kiuchi, "Low temperature chemical vapor deposition method utilizing an electron cyclotron resonance plasma," *Jpn. J. Appl. Phys.*, vol. 22, pp. L210–L212, 1983.
[23] S. Bae, D. G. Farber, and S. J. Fonash, "Characteristics of low-temperature silicon nitride (SiN_x:H) using electron cyclotron resonance plasma," *Solid-State Electron.*, vol. 44, pp. 1355–1360, 2000.
[24] H. Nishi, T. Tsuchizawa, T. Watanabe, H. Shinojima, S. Park, K. Rai, K. Yamada, and S. Itabashi, "Monolithic integration of a silica-based arrayed waveguide grating filter and silicon variable optical attenuators based on p-i-n carrier-injection structures," *Appl. Phys. Exp.*, vol. 3, p. 102203, 2010.
[25] G.-L. Bona, R. Germann, and B. J. Offrein, "SiON high-refractive-index waveguide and planar lightwave circuits," *IBM J. Res. Develop.*, vol. 47, pp. 239–249, 2003.
[26] T. Fuyuki, T. Saitoh, and H. Matsunami, "Low-temperature deposition of hydrogen-free silicon oxynitride without stress by the remote plasma technique," *Jpn. J. Appl. Phys.*, pp. 2247–2250, 1990.
[27] O. Mitomi, K. Kasaya, and H. Miyazawa, "Design of a single-mode tapered waveguide for low-loss chip-to-fiber coupling," *IEEE J. Quantum Electron.*, vol. 30, pp. 1787–1793, 1994.

Hidetaka Nishi received the B.S. and M.S. degrees in mechanical science and engineering from Tokyo Institute of Technology, Japan, in 2005 and 2007, respectively.

In 2007, he joined NTT Microsystem Integration Laboratories, Atsugi, Japan, where he has been engaged in research on silicon-, silica-, and germanium-based optoelectronics devices and their integration technology. Recently, he served concurrently as a senior researcher of Photonics Electronics Technology Research Association (PETRA), Japan and as a research engineer of Nanophotonics center, NTT Corp., Japan. Mr. Nishi is a member of the Optical Society of America and the Japan Society of Applied Physics.

Tai Tsuchizawa received the B.S. and M.S. degrees in physics from Sophia University, Tokyo, Japan, in 1984 and 1986, respectively, and the Ph.D. degree from the University of Tokyo, Japan, in 1990. He was a Senior Research Engineer in NTT Microsystem Integration Laboratories, Atsugi, Japan, where, he is engaged in studies on electron cyclotron resonance (ECR) plasma technology and its application to an etching process for microfabrication. His research interests include fabrication technologies for silicon-based optoelectronics devices. Dr. Tsuchizawa is a Member of the Japan Society of Applied Physics.

Hiroyuki Shinojima received the B.S. and M.S. degrees in applied physics from the Tokyo Institute of Technology, Japan in 1984 and 1986, respectively, and the Ph.D. degree from Muroran Institute of Technology, Japan, in 2009. From 1986 to 2012, he was a Senior Research Engineer at NTT Laboratories, Atsugi, Japan. Currently, he is a Professor of Department of Physics in Liberal Arts in Kurume National College of Technology, Kurume, Japan, where he is engaged in studies on material physics and nonlinear optics in semiconductor microcrystals. His research interests include coherent control in silicon, material physics in low-dimensional semiconductors, and the origin of homo-chirality in terrestrial bio-organic compounds.

Toshifumi Watanabe received the B.S. and M.S. degrees in applied physics from Tokyo Institute of Technology, Japan, in 1982 and 1984, respectively. Currently, he is a Senior Research Engineer in NTT Microsystem Integration Laboratories, Atsugi, Japan where, he is engaged in layout processing studies for electron-beam pattern writers and for computer-aided design data modulation for large-scale integration and photonic circuits. His research interests include robust processing algorithms for very complex pattern layouts. Currently, he is a Senior Engineer with NTT Advanced Technology Corporation.

Sei-Ichi Itabashi received the B.S. and M.S. degrees in physics from Tohoku University, Sendai, Japan, in 1982 and 1984, respectively, and the Ph.D. degree from Hokkaido University, Sapporo, Japan, in 1998. He was a Senior Research Engineer supervisor with NTT Microsystem Integration Laboratories, Atsugi, Japan. In NTT's laboratories, he has engaged in studies on X-ray and EUV optics. And he has also engaged in Silicon photonics. Currently, he is a Senior Engineer with NTT Advanced Technology Corporation. Dr. Itabashi is a member of the Japan Society of Applied Physics.

Rai Kou (M'13) received the B.E. and M.E. degrees in applied physics from Waseda University, Tokyo, Japan, in 2007 and 2009, respectively. From 2007 to 2009, he was a Visiting Researcher at the National Institute for Materials Science (NIMS), Tsukuba, Japan, where he was engaged in nonlinear optics. He has been at NTT Microsystem Integration Laboratories since 2009, and NTT Nanophotonics Center since 2012 (concurrent post), Atsugi, Japan. His current research interests focus on modulation, demodulation and large-scale O/E integration with silicon and its related materials. Mr. Kou is a Member of the Japan Society of Applied Physics (JSAP), the Institute of Electronics, Information and Communication Engineers (IEICE), and IEEE.

Hiroshi Fukuda (M'11) received the B.E. and M.E. degrees in nuclear engineering from Tohoku University, Sendai, Japan, in 1993 and 1995, respectively. In 1995, he joined the NTT Microsystem Integration Laboratories, Atsugi, Japan, where he has been engaged in research on microphotonics devices. Mr. Fukuda is a Member of the Japan Society of Applied Physics, the Institute of Electronics, and Information and Communication Engineers (IEICE) of Japan.

Koji Yamada (M'08) He received the B.E., M.E., and Ph.D. degrees in nuclear engineering from Kyushu University, Fukuoka, Japan, in 1986, 1988, and 2003, respectively. Currently, he is a Senior Research Engineer, Supervisor, and a Distinguished technical member in NTT Microsystem Integration Laboratories, where he has been engaged in theoretical and experimental studies on beam dynamics in electron synchrotrons. Since 2000, he has also been engaged in research on silicon-based photonic systems. He is a member of the Japan Society of Applied Physics, the Atomic Energy Society of Japan, the Particle Accelerator Society of Japan, the Institute of Electronics, Information and Communication Engineers (IEICE), and IEEE.